Study of the heat transport capacity of a novel gravitational loop heat pipe

Xingxing Zhang[1*], Xudong Zhao[1], Jihuan Xu[2] and Xiaotong Yu[3]

[1]*Institute of Energy and Sustainable Development, De Montfort University, Leicester, UK*
[2]*Shanghai Pacific Energy Centre, Shanghai, China;* [3]*Shanghai Solar Energy Research Centre, Shanghai, China*

Abstract

This article presented a theoretical analysis of the heat transfer limits associated with a gravitational loop heat pipe (LHP), which involves the utilization of an innovative liquid feeding/distributing and vapour/liquid-separating structure. The mathematical equations governing the heat transport capacity were applied to simulate several commonly known heat transfer limits of the pipe, namely, viscous, sonic, entrainment, capillary, boiling and liquid filling mass limits. This will allow the determination of the actual figure of the limitation and analyses of the factors effecting the limits, including the loop operational temperature, wick type, evaporator diameter/length, evaporator inclination angle, vapour column diameter in the three-way fitting, liquid filling mass and evaporator-to-condenser height difference. During the study, the heat-transfer limits associated with the three-way fitting for liquid feeding/distribution and vapour/liquid separation were given particular attention. The results derived from the analytical model indicated that the compound screen mesh wick can achieve better thermal performance over the sintered powder and open rectangular groove wicks. It was also found that the heat transport capacity of such LHP operation is positively proportional to the operational temperature, evaporator diameter, evaporator inclination angle, vapour column diameter within the three-way fitting, liquid filling mass and evaporator-to-condenser height difference, and in a reciprocal order to the evaporator length. With the specified loop configuration and operational conditions, the LHP can achieve a high heat transport capacity of around 900 W. Overall, the work presented in this article provided an approach to determine the heat transfer limitations for such a specific LHP operation that will be of practical use for the associated system design and performance evaluation.

Keywords: gravitational; loop heat pipe; feeding structure; heat transfer; limit

*Corresponding author:
x.zhang@dmu.ac.uk

1 INTRODUCTION

Loop heat pipe (LHP) is a two-phase heat-transfer device with the working fluid circulating across a structured loop, which is claimed to be able to provide an enhanced heat transfer at a relatively long-running distance. The occurrence of the LHP was a response to challenges of the increasing desires for efficient thermal controls of satellites, spacecrafts, electronics and cooling/heating systems [1–4]. The first LHP was developed and tested in 1972 by Gerasimov *et al.* [5, 6]. Thereafter, Maydanik [7] Maydanik *et al.* [8] extended the investigation of several specified LHP systems using the basic heat transfer principle. Hamdan *et al.* [9, 10] reported the optimal parameters for a flat-evaporator-equipped LHP and they concluded that a flat evaporator was more convenient for utilization in electronic cooling than the cylindrical evaporators. Li *et al.* [11] aimed to improve the heat transport capacity of a copper/water compact miniature LHP through optimization of the geometrical configuration of its evaporator. Lu *et al.* [12] analyzed the performance of an LHP cooling device for high-power light-emitting diode (LED) package and suggested that the developed LHP was able to effectively control the junction temperature of high-power LED systems. Alklaibi [13] studied several possible configurations of incorporating the LHP into the air-conditioning system to enable the reheat process and concluded that the systems selected in his research were able to achieve a higher coefficient of system performance than the conventional types. Zhao *et al.* [14] recently investigated the feasibility of incorporating an LHP into the solar collectors for use in domestic water heating. They concluded that this integration could obtain enhanced solar heat conversion efficiency over the traditional solar collector systems when using the water/glycol mixture as an anti-freezing working fluid.

The above studies have demonstrated the growing attraction of LHPs for use in practical heat-transporting applications. Compared with those conventional heat transfer methods, the LHP can transport a greater amount of heat at a relatively lower temperature level owing to its evaporation/condensation operation occurring at the evacuated state and the separation of vapour/liquid flow by using different transportation lines, which diminish the effect of entrainment between the two phase fluids towards the heat transfer of the system. Nevertheless, conventional gravitational LHPs face a common problem that lies in the evenness of the liquid distribution on the heat absorbing surface. In a conventional gravitational LHP, liquid is always returned to the heat pipe evaporator, filling up a certain height of the evaporator and being lifted higher via the capillary effect of the pipe. However, sufficient capillary force is not found to lift the liquid to the whole section of evaporator, which is limited to 0.5 m on most occasions [15]. In that case, upper part of the evaporator wick would stay dry, which would cause reduced heat transfer.

To overcome the uneven liquid distribution problem, the top feeding approach has been recently proposed by the authors and to enable this, a three-way feeding and vapour/liquid separation structure has also been developed. This structure was supposed to provide an even distribution of the liquid across the evaporator wick surface, which would ensure enhanced heat transfer. On the basis of the new structure, the heat transport capacity (heat transfer limit) of the LHP operation was investigated theoretically, which gave quantitative figures of the system heat transfer limits and suggested favourite structural and operational configurations. The analyses therefore led to an approach to undertake system design and performance evaluation, and is of direct use for promoting the application of such an LHP system in solar heating projects.

2 DESCRIPTION OF THE LHP OPERATION

A schematic of the LHP operation with the thermal and hydrodynamic couplings is shown in Figure 1. Apart from the separated vapour and liquid transporting lines which separate liquid and vapour flows while in movement, this system also incorporates a unique three-way fitting with an expender to provide even/speedy liquid distribution across the evaporator wick surface, as shown in Figure 2. This three-way fitting enables the connection of the LHP evaporator and vapour/liquid transporting lines. With the tight compression of the expander edge against the evaporator wick, liquid will be slowly and evenly distributed across the wick surface in the evaporator, and the speed of the liquid film falling will be controlled by the height of liquid within the three-way fitting and further by the valve fitted on the liquid returning (transporting) line. Along with the liquid distribution, the evaporator receives the solar radiation striking on the evaporator surface, converting it into the heat which is transferred into inside of the pipe and causes evaporation of the liquid film along the wick surface, while the evaporated liquid, in the form of vapour, will flow upward through the evaporator core space and three-way fitting and enter the vapour transporting line and then the condenser. In the condenser, the vapour is turned to liquid by releasing heat to the passing working liquid, i.e. water, and flows back to the evaporator through the liquid transporting line. This cycle thus leads to the completion of solar heat collection/transportation and water heating process.

Ideally, the liquid flowing across the wick can be instantly evaporated without or with little reservation at the bottom of the LHP evaporator, which would help maximize the heat transport capacity of the LHP. This operation can create an even distribution of the liquid across the evaporator wick surface and therefore lead to enhanced heat transfer over the conventional LHP systems. The first set of such an LHP system is characterized using the dedicated selected parameters shown
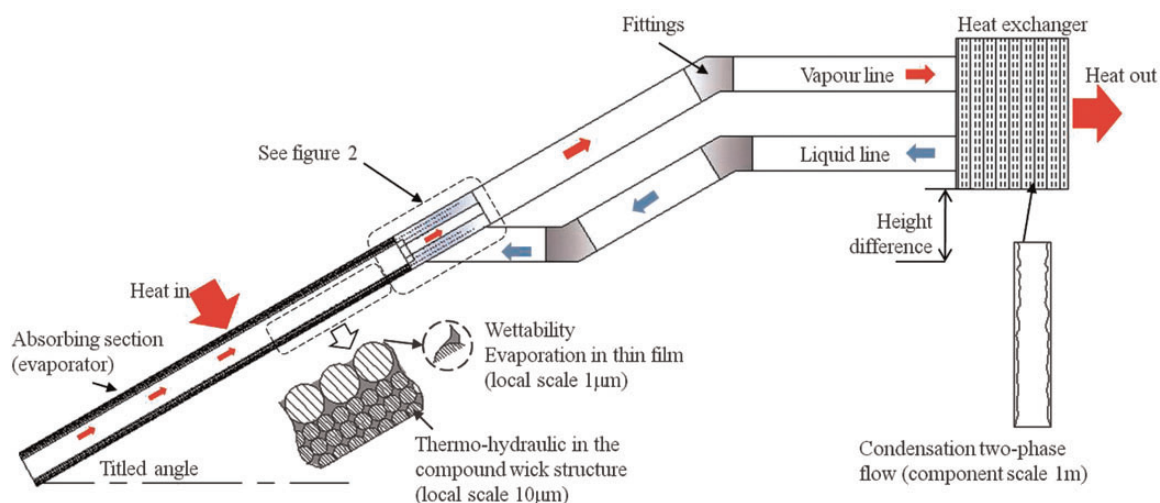
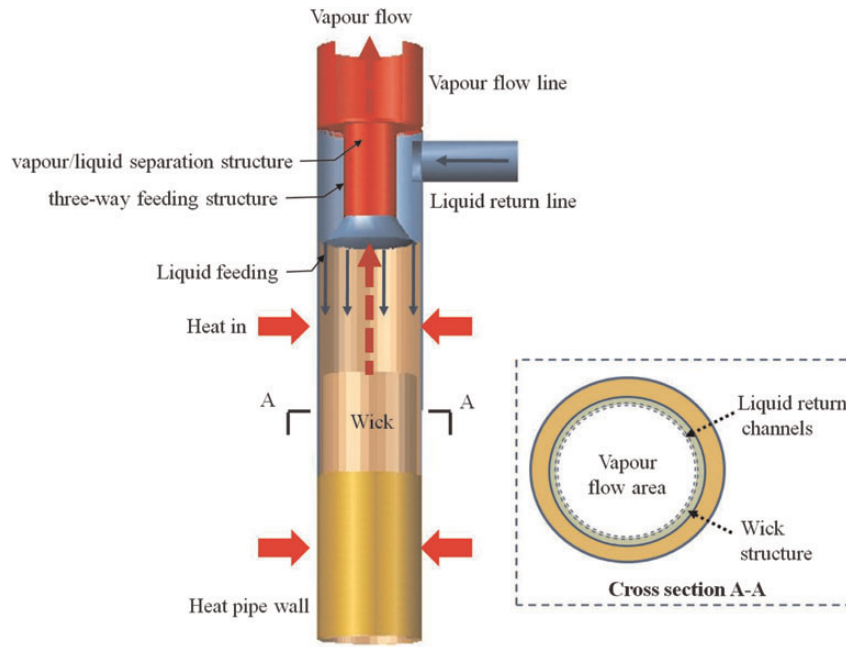**Figure 1.** *Schematic of the thermal and hydrodynamic couplings within the LHP.*

Figure 2. *Schematic of three-way feeding and vapour/liquid separation structure.*

Table 1. *Design parameters of the LHP operation and heat exchanger.*

Parameters	Nomenclature	Value	Unit
External diameter of evaporator	$D_{hp,o}$	0.022	m
Internal diameter of evaporator	$D_{hp,in}$	0.0196	m
Internal diameter of vapour column (three-way fitting)	D_{vt}	0.014	m
Thermal conductivity of evaporator wall	K_{hp}	394	W/mk
Operating temperature range	t_v	20–60	°C
Operating presssure in heat pipe	P_{hp}	1.3×10^{-4}	Pa
Evaporator length	$L_{hp,e}$	1.5	m
Evaporator-to-condenser height difference	H_{hx-hp}	0.3	m
Liquid filling mass	m_f	0.03	kg
Transportation line outer diameter	$D_{ltl,o}/D_{vtl,o}$	0.022	m
Transportation line inner diameter	$D_{ltl,in}/D_{vtl,in}$	0.0196	m
Transportation line length	L_{ltl}/L_{vtl}	1.0/0.9	m
Heat exchanger plate thickness	δ_{hx}	0.00235	m
Heat exchanger plate height	H_{hx}	0.206	m
Heat exchanger plate cluster width	W_{hx}	0.076	m
Heat exchanger plate cluster length	L_{hx}	0.055	m
Heat exchanger plate conductivity	K_{hx}	16.28	W/mk
Heat exchanger number of plate	n_{hx}	20	—
Heat exchanger operating temperature range	t_{hx}	−160 to 225	°C
Heat exchanger operating pressure range	P_{hx}	0–3.24	MPa

Table 2. *Alternative wick structures in the LHP evaporator.*

Parameters		Nomenclature	Value	Unit
Mesh screen	Wire diameter (layer I)	$D_{owi,ms}$	7.175×10^{-5}	m
	Layer thickness (layer I)	$\delta_{owi,ms}$	3.75×10^{-4}	m
	Mesh number (layer I)	$n_{owi,ms}$	6299	/m
	Wire diameter (layer II)	$D_{iwi,ms}$	12.23×10^{-5}	m
	Layer thickness (layer II)	$\delta_{iwi,ms}$	3.75×10^{-4}	m
	Mesh number (layer II)	$n_{iwi,ms}$	2362	/m
	Conductivity	$K_{s,ms}$	394	W/mk
Sintered powder	Pore diameter	$D_{po,sp}$	4.47×10^{-5}	M
	Layer thickness	$\delta_{wi,sp}$	7.5×10^{-4}	M
	Porosity	$\varepsilon_{wi,sp}$	0.64	—
	Layer number	$n_{wi,sp}$	1	—
	Conductivity	$K_{s,sp}$	16.3	W/mk
Rectangular groove	Groove depth	$\delta_{wi,g}$	7.62×10^{-4}	M
	Groove width	$w_{wi,g}$	4.57×10^{-4}	M
	Groove number	$n_{wi,g}$	44	—
	Conductivity	$K_{s,g}$	394	W/mk

in Table 1, while Table 2 gives the alternative selection of the wick structures in the LHP evaporator.

3 ANALYTICAL MODEL SET-UP

During the model set-up, the condenser, as the flat-plate heat exchanger, is assumed to have no restriction on the heat transfer of the system owing to its established heat transfer performance. In that case, the system heat transport capacity will be governed by six limits, i.e. viscous, sonic, entrainment, capillary, boiling and liquid filling mass limits; the minimum values of these limitations will be the actual restraint of the system heat transfer. The magnitudes of these limits are directly related to the thermal properties of the working fluids, wick structures, heat pipe dimensions and operating conditions, and are mathematically illustrated as follows.

3.1 Viscous limit, Q_{VL}

At a low-temperature operation, the viscous forces dominate the performance of the vapour flow. This limit reflects the level

of vapour flow (Q_{VL}) for carrying heat [16]. Busse *et al.* [17] initially developed an equation for computing the viscous limit, which is expressed as:

$$Q_{VL,e} = \frac{\pi D_{v,e}^4 h_{fg} \rho_v P_v}{256 \mu_v L_e} \tag{1}$$

where $Q_{VL,e}$ is the viscous limit at the evaporator (W); $D_{v,e}$ and L_e are the diameter and length of vapour space at the evaporator; h_{fg}, ρ_v, μ_v and P_v are the thermodynamic properties of the vapour at certain operating temperature, respectively, which are the latent heat of vaporization, density (kg/m³), dynamic vapour viscosity (kg/ms) and corresponding saturated vapour pressure (Pa). Table 3 presents the properties of water at some temperature levels. It should be noted that the thermodynamic properties of this water/glycol mixture can be approximately considered the same as water as the glycol only accounts for <5% of the total liquid volume.

This limit should be further applied to other system components, by replacing the evaporator's parameters (diameter and length) with the respective characteristic parameters (diameter and length) of other components, e.g., vapour column diameter in the three-way fitting ($Q_{VL,vt}$), vapour transporting line ($Q_{VL,vtl}$) and heat exchanger ($Q_{VL,hx}$, LHP condenser). Thus, the minimum value among these items would be the ultimate system's viscous limit:

$$Q_{VL} = \min(Q_{VL,e}, Q_{VL,vt}, Q_{VL,vtl}, Q_{VL,hx}) \tag{2}$$

It is found that the viscous limit is only related to three factors, i.e. diameter and length of the vapour space, the characteristic properties of the working fluid, and is irrelevant to wick geometry and structure.

3.2 Sonic limit, Q_{SL}
At higher temperature operation, the Mach number for vapour will significantly increase, especially when the vapour velocity is close to the sonic or supersonic level, the compression state of vapour should be taken into consideration when evaluating its heat transfer capacity. The heat pipe may be choked by the high-speed vapour flow that will limit the total heat transfer capacity in the pipe. The expression for this limit in the

evaporator is given by [16]:

$$Q_{SL,e} = \left(\frac{\pi D_{v,e}^2 \rho_v h_{fg}}{4}\right)\left[\frac{\gamma_v R_v T_v}{2(\gamma_v + 1)}\right]^{0.5} \tag{3}$$

where $Q_{SL,e}$ is the sonic limit (W) at the evaporator; γ_v is the vapour-specific heat ratio whose magnitude is 4/3 for polyatomic working liquid (water); T_v is the average vapour temperature (Kelvin unit) in the absorbing section; R_v is the vapour constant, given by:

$$R_v = \frac{R_0}{m} \tag{4}$$

where R_0 is the universal gas constant ($R_0 = 8.314$ kJ/kmol k); m is the molecular weight of the vapour ($m = 18$ kg/kmol for water).

In this heat pipe, the sonic limit (Q_{SL}) may also occur at the places where vapour flow exists, including the vapour column diameter in the three-way fitting ($Q_{SL,vt}$), vapour transporting line ($Q_{SL,vtl}$) and LHP condenser ($Q_{SL,hx}$). These figures can be calculated by substituting evaporator's parameters with the characteristic diameter for other individual sections. The final system sonic limit can be taken as the minimum value of above items:

$$Q_{SL} = \min(Q_{SL,e}, Q_{SL,vt}, Q_{SL,vtl}, Q_{SL,hx}) \tag{5}$$

Similarly, the wick geometry and structure will not influence the sonic limit, while the vapour core diameter and the characteristic properties of working fluid will impose influence on the limit. For most LHP operations, the effect of the sonic limit is temporary, and will disappear when the operational temperature goes upon to a high level [18].

3.3 Entrainment limit, Q_{EL}
The opposite flow directions of liquid and vapour may result in a shear force at the liquid–vapour interface. When the vapour velocity is sufficiently high, the liquid will be torn from the wick surface and entrained into the vapour [16]. The entrainment can lead to a sudden substantial increase in fluid circulation and consequently immediate dry out of the wick at

Table 3. *The properties of water at different temperatures [23–25].*

t_v (°C)	h_{fg} (kJ/kg)	P_v (Pa)	ρ_v (kg/m³) (e−02)	ρ_l (kg/m³)	K_l (W/k m)	μ_v (kg/ms) (e−06)	μ_l (kg/m s) (e−04)	Σ (N/m) (e−02)
20	2454	2337	1.73	998	0.600	8.84	10.00	7.28
25	2442	3172	2.38	997	0.613	9.03	8.70	7.20
30	2430	4242	3.04	996	0.621	9.22	8.03	7.12
35	2418	5622	4.08	994	0.627	9.42	7.16	7.04
40	2407	7375	5.12	992	0.634	9.62	6.45	6.96
45	2395	9582	6.71	990	0.64	9.82	5.98	6.88
50	2393	12335	8.30	988	0.645	10.00	5.53	6.79
55	2371	15740	10.70	986	0.650	10.20	5.09	6.71
60	2358	19920	13.00	983	0.654	10.40	4.71	6.62

the evaporator, which will effectively decrease the heat transport capacity of the system. In this case, since the liquid and vapour flows separately in the three-way fitting and transporting lines, the entrainment limit may only happen in the evaporator ($Q_{EL,e}$) and heat exchanger. This treatment method, regarded as the unique merit of an LHP, could largely reduce the flow resistance and therefore increase the heat transport capacity of the system. The expression of this limit at the evaporator section is written as:

$$Q_{EL,e} = \left(\frac{\pi D_{v,e}^2 h_{fg}}{4} \right) \left[\frac{\sigma \rho_v}{2 r_{h,s}} \right]^{0.5} \qquad (6)$$

where σ is the surface tension coefficient of water; $r_{h,s}$ is the hydraulic radius of wick surface pore, for a screen mesh wick, which is given by [16]:

$$r_{h,s} = \left(\frac{1}{n_{iwi,ms}} - D_{iwi,ms} \right) / 2 \qquad (7)$$

where $n_{iwi,ms}$ and $D_{iwi,ms}$ are mesh number and wire diameter of the inner screen layer, respectively.

For a sintered powder wick, the hydraulic radius of surface pore is written as [16]:

$$r_{h,s} = \frac{D_{po,sp}}{2} \qquad (8)$$

where $D_{po,sp}$ is the pore diameter in the sintered powder wick structure.

For an open rectangular groove wick, the pore hydraulic radius is [16]:

$$r_{h,s} = w_g \qquad (9)$$

where w_g is the groove width.

For the entrainment limit in the LHP condenser, the same equation can be used by substituting with the structural parameters of the heat exchanger and the hydraulic radius of liquid film. Hence, the smaller limit value between the evaporator and the heat exchanger ($Q_{EL,hx}$) will be the final entrainment limit (Q_{EL}), expressed as:

$$Q_{EL} = \min(Q_{EL,e}, Q_{EL,hx}) \qquad (10)$$

It is found that the entrainment limit varies with not only the heat pipe diameter and the characteristic properties of the working fluid, but also the wick structures and the liquid film in the condenser.

3.4 Capillary limit, Q_{CL}

The capillary limit represents the ability of the heat pipe wicks to carry over the maximum liquid flow for heat transfer. The larger volume liquid pumped by the wicks, the higher heat transport capacity the heat pipe would have [19]. In a heat pipe operation, the maximum capillary pumping head ($\Delta P_{c,max}$) must be greater than or at least equal to the total
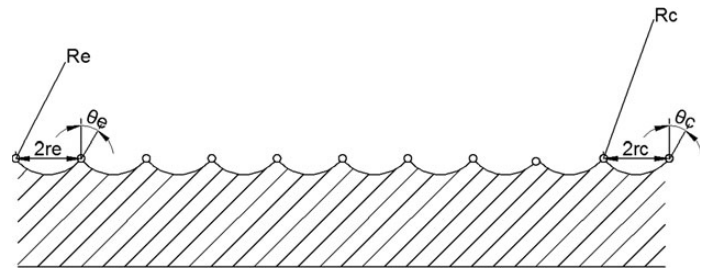

Figure 3. *Wick and pore parameters in evaporator and condenser [3].*

pressure drops along the heat pipe. The pressure drops consists of three aspects [16]: viscous and inertial drop in the vapour (ΔP_v); viscous drop in the liquid (ΔP_l); the gravitational head (ΔP_G) which contains the radial and axial hydrostatic pressure drops (ΔP_{rG} and ΔP_{aG}). In this particular design, the heat pipe works at a gravity-assisted condition and as a result, the overall gravitational head is positive. The pressure relationship can hereby be characterized as:

$$\Delta P_{c,max} + \Delta P_G \geq \Delta P_v + \Delta P_l \qquad (11)$$

From this expression, the capillary limit for the heat transfer is obtained. Each pressure head/drop addressed in the above equation is discussed in sequence as follos:

3.4.1 The maximum capillary head ($\Delta P_{c,max}$)

The capillary pressure power across a curved liquid–vapour interface achieves the maximum value when the contact angle in the evaporator (θ_e) equals zero and that in the condenser (θ_c) is $\pi/2$ (see Figure 3). In this case, the maximum capillary pressure is given by the relation [16]:

$$\Delta P_{c,max} = \frac{2\sigma \cos(\theta)}{r_e} \qquad (12)$$

where r_e is the effective capillary radius which has the different expressions with wick structures, for a compound mesh screen wick [16, 19],

$$r_e = \frac{1}{2 n_{owi,ms}} \qquad (13)$$

where $n_{owi,ms}$ is the mesh number of the outer screen layer.

For a sintered powder wick [16],

$$r_e = \frac{0.41 D_{po,sp}}{2} \qquad (14)$$

For an open rectangular grooves wick [16],

$$r_e = w_g \qquad (15)$$

However, Zhao [19] recommended that the contact angle (θ) should be assumed at $\pi/3$ for a practical heat pipe application. And, Imura *et al.* [20] suggested the theoretical maximum

capillary force should be multiplied by an amendment ratio of 2/3 for a practical mesh-screen wicked heat pipe design.

3.4.2 The gravity pressure head (ΔP_G)

Indeed, if a heat pipe works at the gravitational field and the circumferential communication of the liquid within the wick is possible, the radial hydrostatic pressure drop has to be taken into consideration, which is an effort of liquid rising towards the direction perpendicular to the heat pipe axis by against the gravity force, written as [16]:

$$\Delta P_{rG} = -\rho_l g D_{v,e} \cos \phi \tag{16}$$

where φ is the evaporator inclination angle; g, the gravity acceleration (9.81 m/s^2). For an open groove wick structure, the radial hydrostatic pressure drop equals zero because the circumferential communication of liquid within this wick structure is impossible.

The positive axial hydrostatic pressure head of the liquid column is generated by the overall height difference between the heat pipe condenser and evaporator bottom. This pressure difference is given by the expression:

$$\Delta P_{aG} = \rho_l g \left(\frac{H_{hx}}{2} + H_{hx-hp} + L_e \sin \phi \right) \tag{17}$$

where H_{hx} is the height of heat exchanger; H_{hx-hp} is the height difference between the heat exchanger and the top of evaporator.

Thus, the overall gravity head is given as:

$$\Delta P_G = \Delta P_{aG} - \Delta P_{rG} \tag{18}$$

3.4.3 The vapour pressure drop, (ΔP_v)

The total vapour pressure drop includes four aspects, i.e. vapour pressure drop at the evaporator ($\Delta P_{v,e}$), vapour column diameter in the three-way fitting ($\Delta P_{v,vt}$), vapour transportation line ($\Delta P_{v,vtl}$) and the condenser section ($\Delta P_{v,hx}$). Thus, the overall vapour drop is identified as [16]:

$$\Delta P_v = \Delta P_{v,e} + \Delta P_{v,vt} + \Delta P_{v,vtl} + \Delta P_{v,hx} \tag{19}$$

Vapour pressure drop in evaporator ($\Delta P_{v,e}$), vapour column diameter within the three-way fitting ($\Delta P_{v,vt}$) and vapour transportation line ($\Delta P_{v,vtl}$). The vapour pressure gradient at the evaporator can be written as [16]:

$$\Delta P_{v,e} = F_{v,e} L_e Q_{CL} \tag{20}$$

where $F_{v,e}$ is the vapour frictional coefficient at the evaporator, defined by [21]:

$$F_{v,e} = \frac{8 C_{v,e} (f_{v,e} Re_{v,e}) \mu_v}{\pi D_{v,e}^4 \rho_v h_{fg}} \tag{21}$$

where $C_{v,e}$ and $f_{v,e}$ are the characteristic parameter and the friction factor at the evaporator, which can be determined once

local axial Reynolds number ($Re_{v,e}$) and Mach number ($M_{v,e}$) are defined. These expressions are given below [16, 21]:

$$Re_{v,e} = \frac{4 Q_{CL}}{\pi D_{v,e} \mu_v h_{fg}} \tag{22}$$

$$M_{v,e} = \frac{4 Q_{CL}}{\pi D_{v,e}^2 \rho_v h_{fg} (R_v t_v \gamma_v)^{0.5}} \tag{23}$$

where t_v is the temperature ($^{\circ}$C); Kraus and Bar-Cohen [22] gave the full expression for $C_{v,e}$ and $f_{v,e}$ with different conditions as follows:

$$\begin{aligned} Re_{v,e} \leq 2300, M_{v,e} \leq 0.2, \\ (f_{v,e} Re_{v,e}) = 16, C_{v,e} = 1.00 \end{aligned} \tag{24}$$

$$Re_{v,e} \leq 2300, M_{v,e} > 0.2,$$

$$(f_{v,e} Re_{v,e}) = 16, C_{v,e} = \left(1 + \left(\frac{\gamma_v - 1}{2} \right) M_{v,e}^2 \right)^{-0.5} \tag{25}$$

$$Re_{v,e} > 2300, M_{v,e} \leq 0.2,$$

$$(f_{v,e} Re_{v,e}) = 0.038, C_{v,e} = Re_{v,e}^{0.75} \tag{26}$$

$$Re_{v,e} > 2300, M_{v,e} > 0.2,$$

$$(f_{v,e} Re_{v,e}) = 0.038, C_{v,e} = \left(1 + \left(\frac{\gamma_v - 1}{2} \right) M_{v,e}^2 \right)^{-0.75} (Re_{v,e})^{0.75} \tag{27}$$

The vapour pressure gradient in the vapour column in the three-way fitting and vapour transportation line can be similarly carried out using the expressions (20)–(27) by substituting the respective characteristic parameters, i.e. diameter and length of the vapour flow within each vapour core space.

Vapour pressure drop in condenser section ($\Delta P_{v,hx}$). As the vapour channels in the heat exchanger have the same structure/geometry and are connected in parallel with the same amount of vapour crossing by, the vapour pressure drop in one plate could represent the pressure loss in the whole condenser section. For a single plate, the vapour pressure drop can be written as [21]:

$$\Delta P_{v,hx} = F_{v,hx} \left(\frac{H_{hx}}{2} \right) \left[\frac{Q_{CL}}{(n_{hx}/2) - 1} \right] \tag{28}$$

where $F_{v,hx}$ is the vapour frictional coefficient in the heat exchanger, which can be similarly determined using equations (21)–(27) by substituting the characteristic hydraulic diameter of vapour core space in the heat exchanger; n_{hx} is the heat exchanger number of plate.

3.4.4 The liquid pressure drop (ΔP_l)

The total liquid pressure drop includes four parts, i.e. liquid pressure drop in the condenser section ($\Delta P_{l,hx}$), liquid

transportation line($\Delta P_{l,ltl}$), liquid three-way feeding structure ($\Delta P_{l,lt}$) and the evaporating section ($\Delta P_{l,e}$). Thus, the overall liquid drop is expressed as [16]:

$$\Delta P_l = \Delta P_{l,hx} + \Delta P_{l,ltl} + \Delta P_{l,lt} + \Delta P_{l,e} \quad (29)$$

Liquid pressure drop in condenser section ($\Delta P_{l,hx}$). The liquid pressure drop in each heat exchanger (LHP condenser) plate channel can represent the total liquid pressure drop in the condenser. For a single plate channel, the liquid pressure drop can be described according to Darcy's law [16]:

$$\Delta P_{l,hx} = F_{l,hx} \left(\frac{H_{hx}}{2}\right) \left[\frac{Q_{CL}}{(n_{hx}/2) - 1}\right] \quad (30)$$

where $F_{l,hx}$ is the liquid frictional coefficient in the heat exchanger, defined as [16]:

$$F_{l,hx} = \frac{4\mu_l}{\pi(D_{hx}^2 - D_{lf}^2)\rho_l h_{fg}} \quad (31)$$

where D_{hx} and D_{lf} are, respectively, the hydraulic diameters of plate and liquid film in the heat exchanger; μ_l and ρ_l are the dynamic vapour viscosity and density of the working liquid.

Liquid pressure drop in the liquid transportation line ($\Delta P_{l,ltl}$) and three-way fitting ($\Delta P_{l,lt}$). The liquid pressure drop in the liquid transportation line is [16]:

$$\Delta P_{l,tl} = F_{l,ltl} L_{ltl} Q_{CL} \quad (32)$$

where L_{ltl} is the length of the liquid transportation line; $F_{l,ltl}$ is the liquid frictional coefficient in the liquid transportation line, defined as [16]:

$$F_{l,ltl} = \frac{4\mu_l}{\pi D_{l,ltl}^2 \rho_l h_{fg}} \quad (33)$$

where $D_{l,ltl}$ is the diameter of liquid core in the liquid transportation line.

The liquid pressure gradient in the three-way feeding structure can be similarly carried out using the expressions (32) and (33) by substituting the respective characteristic parameters, i.e. the cross-sectional area and length of the feed liquid flow.

Liquid pressure drop in evaporator ($\Delta P_{l,e}$). The liquid pressure drop at the evaporator is written [16]:

$$\Delta P_{l,e} = F_{l,e} L_e Q_{CL} \quad (34)$$

where $F_{l,e}$ is the liquid frictional coefficient at the evaporator, given as [16]:

$$F_{l,e} = \frac{\mu_l}{K_p A_w \rho_l h_{fg}} \quad (35)$$

where A_w is the cross-sectional area of the liquid flow at the wick; K_p is the wick permeability, which varies with different types of wick structures.

For a compound mesh screen wick structure, the returned liquid flow resistance can be approximately calculated depending on the inner screen layer [16, 19],

$$A_w = \frac{\pi(D_{iwi,in}^2 - D_{v,e}^2)}{4} \quad (36)$$

where $D_{iwi,in}$ is the diameter of the inner screen layer at the evaporator.

$$K_p = \frac{D_{iwi,ms}^2 \varepsilon_{iwi,ms}^3}{122(1 - \varepsilon_{iwi,ms})^2} \quad (37)$$

where $\varepsilon_{iwi,ms}$ is the porosity of the inner mesh screen layer, written as [16]:

$$\varepsilon_{iwi,ms} = 1 - \frac{1.05\pi n_{iwi,ms} D_{iwi,ms}}{4} \quad (38)$$

For a sintered powder structure, the expression of the liquid flow area at the evaporator is the same as that of a mesh screen wick while the permeability of such a wick type is different [16]:

$$K_p = \frac{D_{po,sp}^2 \varepsilon_{sp}^3}{150(1 - \varepsilon_{sp})^2} \quad (39)$$

where ε_{sp} is the porosity of the sintered powder. For an open rectangular grooves structure [16],

$$A_w = \pi(D_{v,e} + \delta_g)\delta_g \quad (40)$$

where δ_g is the groove depth.

$$K_p = \frac{2\varepsilon_g r_{hl,g}^2}{(f_l Re_l)} \quad (41)$$

where $r_{hl,g}$ is the groove hydraulic radius, ε_g is the porosity of the grooves wick; and can be given by [16]:

$$\varepsilon_g = \frac{n_g w_g}{\pi(D_{v,e} + \delta_g)} \quad (42)$$

where n_g is the grove number and $r_{hl,g}$ is expressed as [16]:

$$r_{hl,g} = \frac{2w_g \delta_g}{w_g + 2\delta_g} \quad (43)$$

The ($f_l Re_l$) factor is the frictional coefficient for laminar flow in the rectangular channels, which can be obtained from Figure 4 [16].
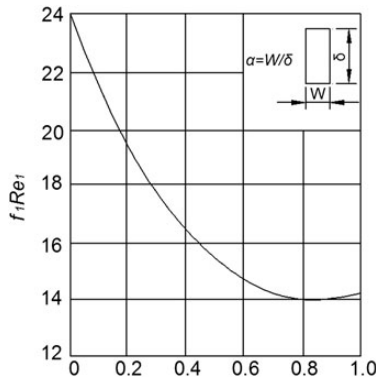
Figure 4. *The frictional coefficients for laminar flow in rectangular tubes* [16].

Combining above equation yields an ultimate expression of the capillary limit:

$$Q_{CL} \leq \frac{\Delta P_{c,max} + \Delta P_G}{(F_{v,e}L_e + F_{v,vt}L_{vt} + F_{v,ltl}L_{ltl} + F_{v,hx}H_{hx}/n_{hx} - 2)} \atop {+(F_{l,e}L_e + F_{l,ltl}L_{ltl} + F_{l,lt}L_{lt} + F_{l,hx}H_{hx}/n_{hx} - 2)} \quad (44)$$

It is observed that the capillary limit is very complicated to determine, varying with not only the heat pipe geometry, operating temperature, working fluid properties, but also the wick types and the plate channel geometry in the heat exchanger.

3.5 Boiling limit, Q_{BL}

The boiling limit (Q_{BL}) represents the maximum radial heat density at the evaporator and the extremely high operating temperature of the heat pipe at which the liquid within certain areas inside of the wicks or wall will be burned out. A similar limitation on peak flux will occur in the condenser (heat exchanger). For the evaporator, an analytical expression can be applied [16]:

$$Q_{BL,e} = \frac{2\pi L_e K_{wi} t_v}{h_{fg}\rho_v \ln(D_{hp,in}/D_{v,e})} \left(\frac{2\sigma}{r_b} - P_{C,max}\right) \quad (45)$$

where $Q_{BL,e}$ is the boiling limit at the evaporator; r_b is the radius of the bubbles, and could be assumed at 2.54×10^{-7} m for the general estimation of a normal heat pipe performance [18]; $P_{C,max}$ is the maximum capillary power, which can be ignored by comparing with the value of $2\sigma/r_b$ [18]; K_{wi} is the effective thermal conductivity of the liquid-saturated wick, for the outer screen layer in cylindrical geometry, which is [16]:

$$K_{wi} = \frac{K_l[(K_l + K_{s,ms}) - (1 - \varepsilon_{owi,ms})(K_l - K_{s,ms})]}{[(K_l + K_{s,ms}) + (1 - \varepsilon_{owi,ms})(K_l - K_{s,ms})]} \quad (46)$$

where K_l and $K_{s,ms}$ are the thermal conductivities of liquid and outer screen layer; $\varepsilon_{owi,ms}$ is the porosity of the inner mesh screen wick layer. The effective thermal conductivity of the

inner screen layer can be similarly obtained from the above equation, thus the overall wick effective conductivity is simply expressed as:

$$K_{wi} = \frac{(K_{owi,ms} + K_{iwi,ms})}{2} \quad (47)$$

For a sintered metal wick with a large contact, K_{wi}, is defined [16]:

$$K_{wi} = \frac{K_l[(2K_l + K_{s,sp}) - 2(1 - \varepsilon_{sp})(K_l - K_{s,sp})]}{[(2K_l + K_{s,sp}) + (1 - \varepsilon_{sp})(K_l - K_{s,sp})]} \quad (48)$$

where $K_{s,sp}$ is the thermal conductivity of solid sintered powder. For the rectangular grooves wick, K_{wi}, is given by [16]:

$$K_{wi} = \frac{(w_f K_l K_{s,g} \delta_g) + w_g K_l(0.185 w_f K_{s,g} + \delta_g K_l)}{(w_g + w_f)(0.185 w_f K_{s,g} + \delta_g K_l)} \quad (49)$$

where $K_{s,g}$ is the thermal conductivity of solid groove; w_f is the groove fin width, defined as [16]:

$$w_f = \frac{\pi(D_{v,e} + D_{hp,in})}{2n_g} - w_g \quad (50)$$

where $D_{hp,in}$ is the diameter of the inner heat pipe wall. For the boiling limit in a heat exchanger ($Q_{BL,hx}$), the same equation can be used by substituting with the equivalent inner diameter and vapour space of the heat exchanger plate. Thus, the smaller limit value between the absorbing area and heat exchanger will be the ultimate entrainment limit, expressed as:

$$Q_{BL} = \min(Q_{BL,e}, Q_{BL,hx}) \quad (51)$$

It is concluded that the boiling limit is not determined by heat pipe geometry, operating temperature or working fluid properties, but the wick structures and the plate geometry in the condenser section.

3.6 Liquid filling mass limit, Q_{FL}

The liquid filling mass limit is the minimum liquid level required to be filled into the loops, which influences the heat transportation capacity through the liquid gravity force. This limit reflects the minimum amount of liquid which is completely circulated in the heat pipe loop with the assistance of gravity at a certain height level. The liquid filling mass limit for the evaporator ($Q_{FL,e}$) is [21]:

$$Q_{FL,e} = \left(\frac{m_f}{xL_e}\right)^3 \frac{K_l g h_{fg}}{3\pi^2 \mu_l \rho_l D_{hp,in}^2} \quad (52)$$

where m_f is the liquid filling mass; x is the parameter relating to the liquid filling mass, 0.8 for pipes with wick structure, 1.0 for those sections without wick. The liquid filling mass limit is
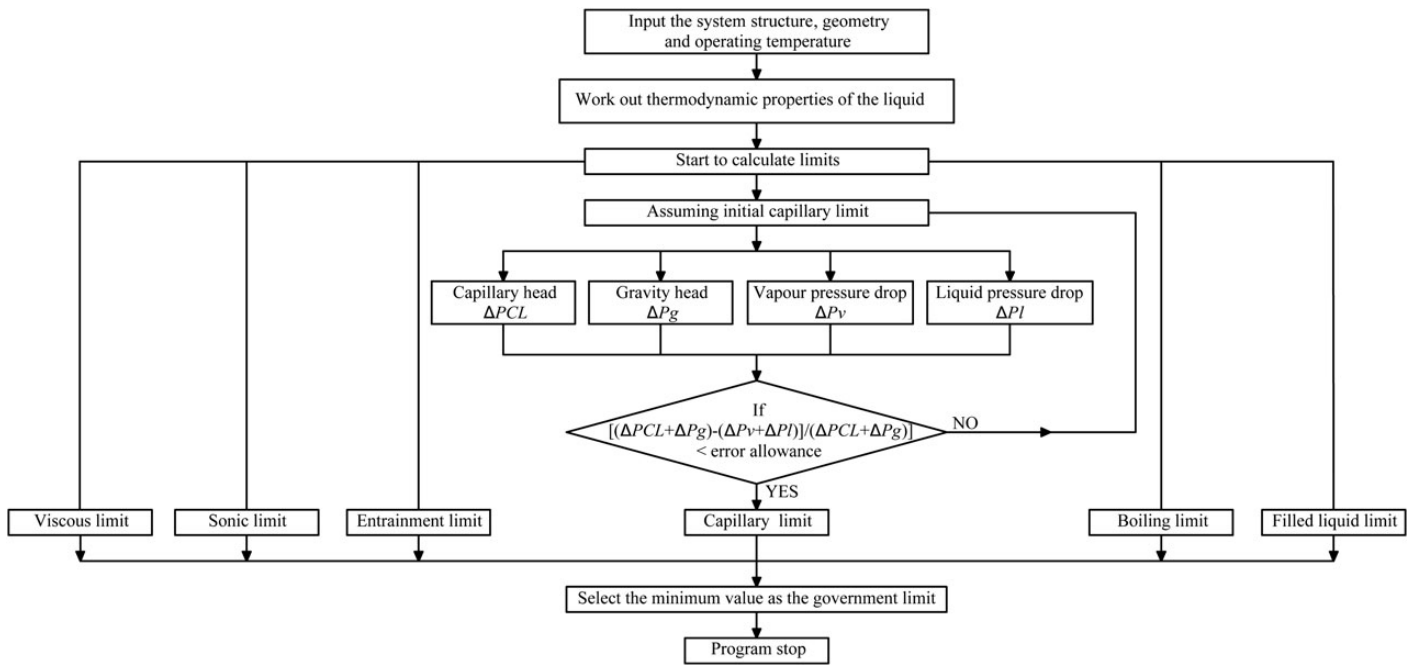
Figure 5. *The computer program flow chart for heat transfer limits.*

influenced by the factors including wick length, heat pipe geometry, operating temperature and working fluid.

3.7 Algorithm for computer model set-up and its validation

The algorithm used for analysing above six limits is described as follows. Figure 5 is the flow chart of the computer programming process.

(i) Given the geometry of LHP system components, technical parameters could be obtained from Tables 1 and 2.

(ii) Given certain system operating temperatures/pressures, the thermodynamic properties of working fluids could be obtained from Table 3.

(iii) Calculating the viscous limits at appropriate regions in the operation, and taking the minimum value as the ultimate viscous limit by Equations (1) and (2).

(iv) Calculating the sonic limits at appropriate regions in the operation, and taking the minimum value as the ultimate sonic limit by Equations (3)−(5).

(v) Calculating the entrainment limits at the wicked absorbing pipes and heat exchanger, and taking the smaller value as the ultimate entrainment limit by Equations (6)−(10).

(vi) Running a numerical iteration to work out capillary limit, Q_{CL}, by Equations (11)−(44)

    (a) Given an initial value of Q_{CL}.

    (b) Capillary pressure, ΔP_{CL}, can be obtained using Equations (12)−(15).

(c) Gravity pressure, ΔP_{rG} and ΔP_{aG}, can be obtained using Equation (16)−(18).

(d) Vapour pressure drop, ΔP_v, can be obtained using Equations (19)−(28).

(e) Liquid pressure drop, ΔP_l, can be obtained using Equations (29)−(43).

(f) If $[(\Delta P_{CL} + \Delta P_G) - (\Delta P_v + \Delta P_l)]/(\Delta P_{CL} + \Delta P_G) < -0.5\%$ (error allowance), then decrease Q_{CL} by 10, and return to step 'b' for re-calculation.

(g) If $[(\Delta P_{CL} + \Delta P_G) - (\Delta P_v + \Delta P_l)]/(\Delta P_{CL} + \Delta P_G) > 0.5\%$ (error allowance), then increase Q_{CL} by 10, and return to step b for re-calculation.

(h) If $-0.5\% \leq [(\Delta P_{CL} + \Delta P_G) - (\Delta P_v + \Delta P_l)]/(\Delta P_{CL} + \Delta P_G) \leq 0.5\%$ (error allowance), heat balance is achieved and real value of Q_{CL} can be obtained.

(vii) Calculating the boiling limits at the wicked evaporator and the heat exchanger, and taking the smaller value as the ultimate boiling limit by Equations (45)−(51).

(viii) Calculating the liquid filling mass limits at the wicked evaporator by Equations (52).

(ix) Taking the minimum value of the above six limits as the governing limit of the whole operation.

(x) Program stops.

It should be noted that this model is a revised version of the simulation model carried out by Zhao *et al.* [21], which has already been proved with its accuracy for predicting the heat pipe thermal performance, this model is therefore believed to

be able to predict the heat pipe limits at a reasonable accuracy.

4 OPERATION OF THE MODEL—IMPACTS OF THE SYSTEM PARAMETERS ON LHP PERFORMANCE

In reality, the LHP performance is dependent upon its operational and geometrical parameters, including loop working temperature, wick types, evaporator diameter/length, evaporator inclination angle, vapour column diameter in the three-way fitting, liquid filling level and evaporator-to-condenser height difference. The impacts of these parameters on the system performance are analysed and presented as follows.

4.1 Impact of the LHP operational temperature
Each vapour pressure level inside the LHP will reflect a corresponding saturated vapour temperature, termed as the operational temperature of the LHP. The vapour pressure of water may be linked to its temperature in the following expression:

$$P = 133.32 \exp\left[20.386 - \frac{5132}{(t + 273.13)}\right] \tag{53}$$

where t and P are the temperature and vapour pressure of water at certain thermodynamic status.

Taking into consideration of the design parameters, i.e. the compound mesh screen as the wick structure, the evaporator internal diameter of 19.6 mm, the evaporator length of 1.5 m, the evaporator inclination angle of 30°, vapour column diameter of 14 mm in the three-way fitting, the liquid filling mass of 0.03 kg, and the evaporator-to-condenser height difference of 0.3 m, the above analytical computer model was run to obtain the results. The relationship between the heat pipe operational temperature and the heat transfer limits were simulated and the results were presented in Figure 6. It was found that the boiling limit decreased with the increasing temperature, while the other five limits increased when the operational temperature grew higher. The capillary limit was found to be the governing limit in this case. A linear correlation between the capillary limit and operating temperature was found. The viscous limit in the three-way feeding structure was observed to be far larger than the corresponding system limitation. This phenomenon could be explained as follows: at higher heat pipe operational temperature, an enhanced evaporation rate of the liquid occurred and as a result, the heat transport capacity of the LHP was increased. Increasing the operational temperature would lead to changing of the thermodynamic properties of the working fluid and this would further create increased fluid turbulence (Reynolds number) within the piping, which would consequently lead to an increased viscous limit. When the operational temperature rises, the sonic limit (occurring in the
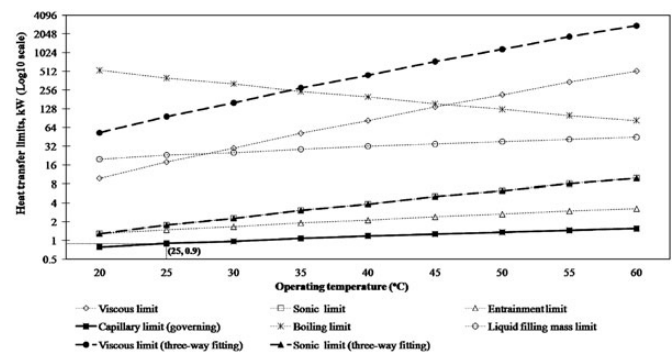

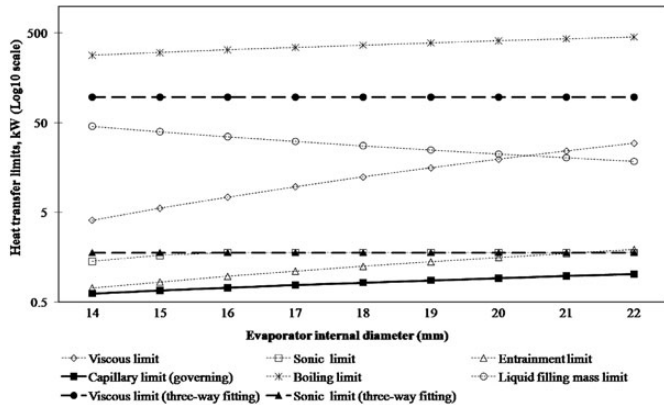Figure 6. *The operational limits varying with operating temperature.*

three-way fitting) will become higher due to the increased vapour density and the larger amount of vapour circulation mass in the loop system. The entrainment limit would also grow larger as a lower shear force would occur at the vapour and liquid boundary within the wicked absorbing pipes. The sufficient vaporization enabled the higher heat transport capacity within the heat pipes to overcome the vapour flow resistance and furthermore, the liquid return resistance was also lowered down owing to the lower liquid flow viscosity while the temperature rises. This behaviour immediately strengthened the overall capillary force. Heat transfer in heat pipes dominated the boiling limit. When the overall liquid vaporization was increased due to the increased temperature, the danger of dry-out of the heat pipe will appear and therefore, the boiling limit would tend to fall, while higher latent heat of liquid vaporization helps to grow the liquid filling mass limit.

4.2 Impact of the wick structure
While keeping the operational temperature, geometrical sizes, evaporator inclination angle, vapour column diameter in the three-way fitting, liquid filling mass level, evaporator-to-condenser height difference and other loop parameters the same, change of the wick structure in the evaporator from screen mesh, sintered powder to the open rectangular groove, will lead to variation of the LHP heat transfer limit, and the correlation among these two variable is presented in Table 4. It is found that the use of the screen mesh wick could obtain the highest heat transport capacity (operating limit) over the other two wicks with this particular design. The critical limits were respectively observed as the entrainment limit for groove wick and capillary limit for the other two wicks. The groove wick has the largest capillary and boiling limit but the smallest entrainment limit. The remaining three limits, i.e. viscous, sonic and liquid filling mass limits, stayed the same for all the wicks. This phenomenon could be explained as follows: the groove wick structure usually has the lowest liquid frictional force and radial heat transfer resistance in a gravity-assisted operation and therefore it should have much higher capillary limit in the same working conditions. The groove wick has a relatively larger pore hydraulic radius and higher wick effective thermal

Table 4. *The analytical results of heat transfer limits with three different wick structures.*

Wick type	Viscous limit (kW)	Sonic limit (kW)	Entrainment limit (kW)	Capillary limit (kW)	Boiling limit (kW)	Liquid filling mass limit (kW)	Governing limit (kW)
Screen mesh	17.93	1.77	1.50	**0.90**	401.29	23.26	**0.90**
Sintered powder	17.93	1.77	2.12	**0.64**	337.71	23.26	**0.64**
Open groove	17.93	1.77	**0.86**	6.92	702.43	23.26	**0.86**

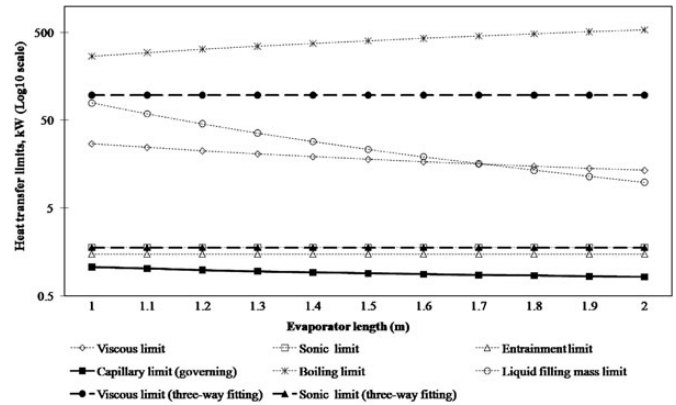**Figure 7.** *The operational limits varying with the internal evaporator diameter.*

Figure 8. *The operational limits varying with the evaporator length.*

conductivity than other two wicks, which would consequently result in higher boiling limit but relatively lower entrainment limit. According to the definitions of viscous, sonic and liquid filling mass limits, the wick structure would not impose an impact to these three limits when having fixed design and operational parameters e.g. loop geometry, vapour core space, operational temperature and working fluid.

4.3 Impact of the evaporator diameter

While keeping the wick structure, heat pipe operational temperature, evaporator length, evaporator inclination angle, vapour column diameter in the three-way fitting, liquid filling mass, evaporator-to-condenser height difference and other loop parameters same, change of the evaporator diameter would lead to a change of the heat transfer limit of the LHP, and their correlation is presented in Figure 7. In this case, only the liquid filling mass limit fell, while the other five limits increased with the increasing evaporator diameter. The capillary limit was found to be the governing limit for this operation, and a linear relation between the capillary limit and the evaporator diameter was found. This phenomenon could be explained as follows: increasing the evaporator diameter would result in a higher Reynolds number, larger amount of liquid evaporation rate, broader vapour/liquid flow space, lower vapour flowing velocity and large amount of liquid to be evaporated within evaporator. These trends of variation will consequently assist in increasing the values of viscous, sonic, entrainment, capillary and boiling limits of the LHP. However,

the sonic limit originally occurred in the evaporator when its diameter was <15 mm and later began to appear in the three-way fitting constantly, and changing the evaporator diameter would not affect this limit any more. As the internal evaporating space was inversely proportional to the liquid filling mass limit, an increased evaporator diameter required more liquid to be filled in and with the current liquid volume, this limit therefore decreased.

4.4 Impact of the evaporator length

While keeping the heat pipe wick structure, operational temperature, evaporator diameter, evaporator inclination angle, vapour column diameter in the three-way fitting, liquid filling mass, evaporator-to-condenser height difference and other loop-related parameters same, change of the evaporator length would lead to a certain level of change in the heat transfer limit of the LHP, and their correlation is presented in Figure 8. In this case, the viscous, capillary and liquid filling mass limits decreased with increasing evaporator length while the boiling limit varied in the opposite trend, and the other two limits remained constant. The capillary limit was also found to be the critical limit for this operation. This phenomenon could be explained as follows: the increased evaporator length represents increased vapour/liquid flow distance within the loop, which led to increased vapour/liquid frictional resistance and possibly decreased volume flow rate (smaller Reynolds number), which thus led to decreased viscous and capillary limits. Since an increased evaporator space requires more liquid to be filled in and at a current liquid level, the liquid filling mass limit
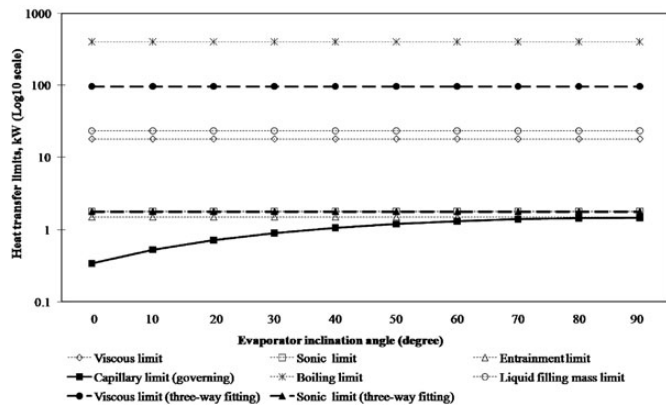
Figure 9. *The operational limits varying with the evaporator inclination angle.*

Figure 10. *The operational limits varying with the vapour column diameter in the three-way fitting.*

hereby reduced. During this process, the boiling limit became larger as the increased evaporator length led to the increase in overall loop volume, evaporation rate of the water and operational temperature. In terms of other limits, the evaporator length could not find an interrelation with them and therefore, caused no impacts on them.

4.5 Impact of the evaporator inclination angle

While keeping the heat pipe wick structure, operational temperature, evaporator diameter/length, vapour column diameter in the three-way fitting, liquid filling mass, evaporator-to-condenser height difference and other loop-related parameters the same, a change of the evaporator inclination angle would lead to a certain level of change in the heat transfer limit of the LHP, and their correlation is presented in Figure 9. In this case, the capillary limit was the critical limit and increased with the evaporator inclination angle while other five limits all remained the same. A smooth logarithmic relation between the capillary limit and the evaporator inclination angle was found and the reason for this was owing to the effect of gravity. The capillary limit significantly increased when the inclination angle varied from 0° to 60°, but then gently grew up to its maximum value. A higher inclination angle led to higher hydrostatic force, which improved the system capability in transporting the returned liquid flow, and thus led to increased heat flux while the other limits have no internal relationship with this factor.

4.6 Impact of the vapour column diameter in three-way fitting

While keeping the heat pipe wick structure, operational temperature, evaporator diameter/length, evaporator inclination angle, liquid filling mass, evaporator-to-condenser height difference and other loop-related parameters the same, a change of the vapour column diameter in a three-way fitting would lead to a certain level of change in the heat transfer limit of the LHP, and their correlation is presented in Figure 10. It is found
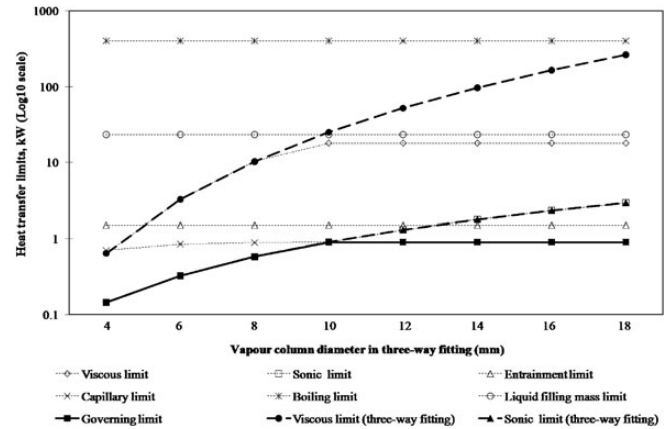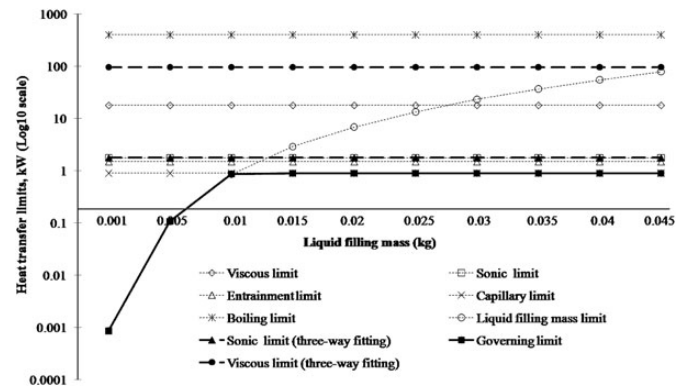

Figure 11. *The operational limits varying with the liquid filling mass level.*

that the viscous, sonic and capillary limits increased with the larger vapour column diameter in the three-way fitting, whereas the other limits remained constant. The system viscous limit appeared in the three-way fitting when the vapour column diameter was <9 mm. In this case, the governing limit varied with operational conditions: the sonic limit, occurring in the three-way fitting, was the critical limit while the vapour column diameter was <10 mm, but the capillary limit followed and became the governing limit when the column diameter was >10 mm. It is therefore concluded that the minimum vapour column diameter in the three-way fitting should be no <10 mm for this LHP operation to avoid the overall heat transfer ability being weakened.

4.7 Impact of the liquid filling mass

While keeping the heat pipe wick structure, operational temperature, evaporator diameter/length, evaporator inclination angle, vapour column diameter in the three-way fitting, evaporator-to-condenser height difference and other loop parameters the same, a change of the heat pipe liquid filling mass would cause a change in the heat transfer limits of the LHP, and their correlation is presented in Figure 11. It is found
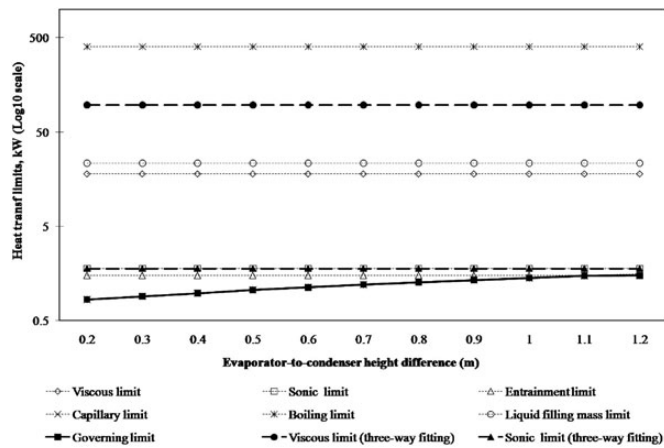
Figure 12. *The operational limits varying with the evaporator-to-condenser height difference.*

that the liquid filling mass limit increased with increasing liquid mass, whereas the other limits remained constant. In this case, the governing limit varied with operational conditions: the liquid filling mass is the governing limit when the mass level was <0.01 kg, but the capillary limit stepped in and became the governing limit when the mass level was >0.01 kg. It is accordingly concluded that the minimum liquid filling mass should be no less than this level for the screen mesh wick operation; otherwise the surface dry-out state will occur within the evaporator.

4.8 Impact of the heat pipe evaporator-to-condenser height difference

While keeping the heat pipe wick structure, operational temperature, evaporator diameter/length, evaporator inclination angle, vapour column diameter in the three-way fitting, liquid filling mass and other loop parameters the same, a change of the heat pipe evaporator-to-condenser height difference would cause a change of the heat transfer limit of the LHP, and their correlation is presented in Figure 12. In this case, the capillary limit increased with the evaporator-to-condenser height difference increasing while other five limits all remained the same. However, the governing limit presents a change with the operational conditions; the capillary limit remained in the dominated position when the height difference was <1.1 m, and the entrainment limit (occurring in the heat exchanger) would become the dominated factor when the difference was >1.1 m. A linear relation between the capillary limit and the height difference was found and the reason for this was owing to the effect of gravity. A higher height difference brought on a higher hydrostatic force, which enhanced the system capability force to deliver the returned liquid flow, and therefore can transfer more applied heat load. The other limits have no relationships with this parameter and remained constant.

5 CONCLUSIONS

By modifying the established computer model, the author carried out the theoretical analysis of the heat transport capacity associated with a novel gravitational LHP with a unique three-way fitting for liquid feeding/distribution and vapour/liquid separation. Six operational limits, including viscous, sonic, entrainment, capillary, boiling and liquid filling mass, were considered and the impact of the various operational and geometrical parameters of the LHP system on its heat transfer limits were investigated. It is concluded that the dedicated structured LHP system can achieve a heat transport capacity of around 900 W at the specified operational condition. Among the three named wick structures, i.e. compound mesh screen, sintered powder and open rectangular groove, the mesh screen was found to present the best heat transfer performance. The approach for determining the heat transfer limitation for such a specific LHP was presented in the form of the analytical model and the results obtained indicated that to gain an improved LHP thermal behaviour, the following methods should be applied: (1) increasing the LHP operational temperature, i.e. 30°C; (2) increasing the evaporator internal diameter, i.e. 22 mm, (3) decreasing the evaporator length, i.e. 1.2 m; (4) increasing the evaporator inclination angle, i.e. 60°; (5) increasing the vapour column diameter in the three-way fitting, i.e. 16 mm; (6) filling more liquid volume into the system, i.e. 0.03 l and (7) uplifting the heat pipe condenser above its evaporator, i.e. 1 m. These addressed approaches and recommendations would help carry out the system design and performance evaluation associated with such an LHP configuration in future practical heat-transfer applications.

REFERENCES

[1] Dunn PD, Reay DA. *Heat Pipes*, 4th edn. Elsevier Science Ltd, 1994.
[2] Advanced Themal Devices, Inc. LHP introduction. <http://www.atdi-web.com/home.php?fn=eng/technology> (12 November 2011, date last accessed).
[3] Yun J, Kroliczek E. Operation of capillary pumped loops and loop heat pipes. <http://china-heatpipe.net/heatpipe04/03/2006-10-1/061018556408_0_32.htm> (12 November 2011, date last accessed).
[4] Launay S, Sartre V, Bonjour J. Parametric analysis of loop heat pipe operation: a literature review. *Int J Ther Sci* 2007;**46**:621–36.
[5] Gerasimov YuF, Maydanik YuF. Heat pipe. USSR Inventors Certificate 449213, 1974.
[6] Gerasimov YuF, Maydanik YuF, Shchogolev GT, *et al*. Low-temperature heat pipes with separate channels for vapor and liquid. *Eng.-Phys. J.* 1975;**28**:957–60 (in Russian).
[7] Maydanik YuF. Review loop heat pipes. *Appl Therm Eng* 2005;**25**:635–57.
[8] Maydanik YuF, Fershtater YuG, Solodovnik N. Loop heat pipes: design, investigation, prospects of use in aerospace technics. SAE Paper 941185, 1994.
[9] Hamdan M, Cytrynowicz D, Medis P, *et al*. Loop heat pipe (LHP) development by utilizing coherent porous silicon (CPS) wicks. In: *Proceedings of the Eighth ITHERM Conference*, 29 May–2 June 2002, pp. 457–65.
[10] Cytrynowicz D, Hamdan M, Medis P, *et al*. Test cell for a novel planar mems loop heat pipe based on coherent porous silicon. In: *Space*

Technology and Applications International Forum, 2–6 February 2003, Albuquerque, New Mexico.

[11] Li J, Wang D, Peterson GP. Experimental studies on a high performance compact loop heat pipe with a square flat evaporator. *Appl Therm Eng* 2010;**30**:741–52.

[12] Lu X-y, Hua T-C, Liu M-j, *et al*. Thermal analysis of loop heat pipe used for high-power LED. *Thermochim Acta* 2009;**493**:25–9.

[13] Alklaibi AM. Evaluating the possible configurations of incorporating the loop heat pipe into the air-conditioning systems. *Int J Refrig* 2008;**31**:807–15.

[14] Zhao X, Wang Z, Tang Q. Theoretical investigation of the performance of a novel loop heat pipe solar water heating system for use in Beijing, China. *Appl Therm Eng* 2010;**30**:2526–36.

[15] Faghri A. *Heat Pipe Science and Technology*, 1st edn. Taylor & Francis Group, 1995.

[16] Chi SW. *Heat Pipe Theory and Practice: A Source Book*. Hemisphere Pub. Corp, 1976.

[17] Busse CA. Theory of ultimate heat transfer limit of cylindrical heat pipes. *Int J Heat Mass Transf* 1973;**16**:169–86.

[18] Zhuang J, Zhang H. *Heat Pipe Technology and Engineering Application*, 1st edn. The Press of Chemistry Industry, 2000.

[19] Zhao X. Analysis and amendment of design factors about heat pipe of screen wicks. *J Nanjing Norm Univ (Engineering and Technology)* 2004;**4**:07–10.

[20] Imura H, Kozai H, Ikeda Y. The effective pore radius of screen wicks [A], Ma Tongze. Advances in Heat Pipe Science and Technology[C]. In: *Proceedings of the 8th International Heat Pipe Conference*, 1992, pp. 113–8.

[21] Riffat SB, Zhao X, Doherty PS. Analytical and numerical simulation of the thermal performance of 'mini' gravitational and 'micro' gravitational heat pipes. *Appl Therm Eng* 2002;**22**:1047–68.

[22] Kraus AD, Bar-Cohen A. *Thermal Analysis and Control of Electronic Equipment*. McGraw-Hill, 1983.

[23] Holman JP. *Heat Transfer*, 5th edn. McGraw-Hill, 1981.

[24] eFunda, Inc., Water properties. <http://www.efunda.com/materials/> (24 September 2011, date last accessed).

[25] The Engineering ToolBox, Water thermal properties. <http://www.engineeringtoolbox.com/> (24 September 2011, date last accessed).